Surface Science 735 (2023) 122322

Contents lists available at ScienceDirect

Surface Science

journal homepage: www.elsevier.com/locate/susc

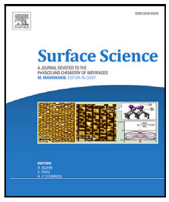

Cu-phthalocyanine long-range ordered bulk growth due to the weak interaction with highly oriented pyrolytic graphite substrate

Daniele Paoloni *, Alessandro Ruocco

Dipartimento di scienze, Università degli studi Roma Tre, Via della Vasca Navale 84, 00146 Rome, Italy

ARTICLE INFO

Keywords:
Phthalocyanine
HOPG
Structural and electronic properties
Organic film ordered growth
Electron energy loss spectroscopy
Electron diffraction

ABSTRACT

We investigate the relationship between the ordered growth of copper-phthalocyanine (CuPc) on highly oriented pyrolytic graphite (HOPG) and the electronic interaction at the interface. Via spot profiles analysis of electron diffraction patterns we determine an ordered growth for all measured CuPc films ranging from sub-monolayer to 3.3 nm. In particular we found that for CuPc thick films the ordered domains have a dimension of 50 nm. Electronic structure of CuPc/HOPG interface was studied by means of photoelectron and electron energy loss spectroscopies (EELS). From photoelectron spectroscopy we observe that molecules at the interface are weakly physisorbed. This weak interaction contributes to the formation of ordered 2-D islands. Since the geometry of the surface unit cell does not change with film thickness, the second CuPc layer grows stacked flat on the first one, forming ordered 3-D islands. It follows that the ordered bulk phase derives from the weak interaction between Pcs and HOPG. The Q band of CuPc/HOPG, measured via EELS, is different from the ones of the most common Pc phases. Therefore, electron diffraction and EELS measurements indicate the formation of a novel Pc long-range ordered structure observed only at this interface.

1. Introduction

Low-cost and flexible electronic devices, like solar cells and transistors, are realized using organic molecules. The properties of these materials depend on molecular film order [1] and crystal structure [2], which can be tuned depositing molecules on different substrates [3]. In particular, a clear correlation between long-range order and larger electron mobility has been demonstrated [1]. Moreover, long-range ordered monolayer phases can be obtained via the substrate templating effect [4]. However, technological applications require long-range order in 3 dimensions and a full comprehension of the relation between the interaction of the first molecular layer and bulk growth is still in progress. In this context, we study electronic structure and morphology of the copper-phthalocyanine (CuPc) deposited on highly oriented pyrolytic graphite (HOPG). CuPc/HOPG interface is a prototype of weak physisorption [5]. Indeed, molecules are free to move [6,7] and, consequently, rearrange on the surface. The early stage of the growth is characterized by chains of molecules with a preferential alignment along the three high symmetry axes of the graphite [6,8]. They are precursors to the formation of ordered two-dimensional (2-D) clusters with both square and parallelogram shape [6], which are obtained heating high coverage samples at 400 °C. This annealing does not remove all the bulk phase 3-D islands [9], which arise before completing the monolayer. To fully characterize the Pc growth on HOPG, we combine photoemission spectroscopy, electron energy loss spectroscopy (EELS) and electron diffraction. We perform EELS at low momentum transfer (the optical limit) to compare our data with the previous optical absorption measurements [10,11], since in the optical limit the two techniques have similar cross sections [12]. Diffraction experiments are performed with a home-built monochromatic electron gun and an electron analyser, which collects the elastically scattered electrons as a function of the sample rotation. This method allows a quantitative analysis of the diffraction pattern; in order to distinguish it from the conventional low-energy electron diffraction (c-LEED), we refer to it as scanning angle-LEED (SA-LEED). SA-LEED is very similar to the well-known spot profile analysis low-energy electron diffraction (SPA-LEED) technique [13]. SA-LEED and SPA-LEED have common features such as a narrower transmission function and a greater dynamic with respect to the conventional LEED [13].

Using SA-LEED, we quantify the long-range order by measuring the size of the in-plane dimension of the coherent scattering domains, called also crystallites [14]. This value has not to be confused with the micron-scale grain size measured using probe and electron mi-

* Corresponding author.
E-mail addresses: daniele.paoloni@uniroma3.it (D. Paoloni), alessandro.ruocco@uniroma3.it (A. Ruocco).

https://doi.org/10.1016/j.susc.2023.122322
Received 20 February 2023; Received in revised form 13 April 2023; Accepted 9 May 2023
Available online 24 May 2023

Table 1
Summary table of the sample studied.

Thickness (Å)	Rate (Å/min)	Grown on top	Used in				
			XPS	UPS	SA-LEED	c-LEED	EELS
1.5	1.2	clean HOPG	x	x	x		
1.5	0.3	clean HOPG					x
5	1.2	clean HOPG	x	x	x	x	
10	0.45	1.5 Å					x
33	1.2	1.5 Å	x	x	x		
40	0.65	10 Å					x

croscopes [9,15]. Indeed, these techniques have not enough resolution to distinguish between different domains inside the same grain at this scale.

The growth on HOPG is compared with the one on Al(100) [16,17], which is characterized by strong Pc chemisorption and electron charge transfer from Al to the molecule [16]. This strong chemisorption gives rise to a disordered α-like phase. Generally, Pcs self-assemble and the distance between molecules depend on the phase. Moreover, the Q band, which is associated to the technological relevant transition between the highest occupied molecular orbital (HOMO) and the lowest unoccupied molecular orbital (LUMO), has a different line shape as a function of the Pc phase. Feng et al. [18] computed that the probability to excite a charge transfer excitation between HOMO and LUMO of two adjacent molecules is dependent on Pc lattice parameters. We apply this model to show that HOPG induces an ordered CuPc growth with a characteristic crystal phase.

2. Material and methods

All measurements were performed at LASEC laboratory (Dipartimento di Scienze, Università degli studi Roma Tre). Samples of CuPc/HOPG were prepared in situ by evaporation from crucible. The chamber pressure was in 10^{-10} mbar range during the evaporation, the crucible temperature was ~385 °C and the sample was at room temperature. Substrate is a ZYA type HOPG with (0.4 ± 0.1)° mosaic spread [19], purchased by SPI. It was prepared in air by peeling the sample with adhesive tape and then annealed in vacuum at 520 °C. CuPc molecules were purchased by Sigma-Aldrich (purity 99%) and further purified in ultra-high vacuum (UHV) for many hours at 200 °C well below the sublimation temperature. The estimation of thickness coverage using X-ray photoemission spectroscopy (XPS) signals ratio between overlayer and substrate [20] is not possible, due to the superposition of C 1s signals of Pc and HOPG and Volmer–Weber growth [9]. For these reasons, overlayer thickness is determined by measuring evaporation rate with a quartz microbalance (Sycon Instruments STM-100/MF), calibrated using the XPS estimation of CuPc/Al(100) samples. Therefore, sample coverages reported are the equivalent Frank–Van der Merwe (FVM) growth thickness. In particular, 1.5 Å thickness corresponds to a sub-ML in a FVM growth.

All the measurements, summarized in Table 1, were performed at room temperature. Photoemission spectra, EELS and SA-LEED patterns were acquired by means of a concentrical hemispherical analyser (CHA) with 66 mm mean radius, which is equipped with a multichannel detector for parallel energy acquisition. Moreover, a conventional back-display low-energy electron diffraction (c-LEED) pattern of 5 Å sample was measured using a commercial Omicron Spectaleed. Ultraviolet photoemission spectroscopy (UPS) and XPS measurements were performed using He I (photon energy $h\nu = 21.2$ eV) and monochromatic Al $K\alpha_1$ ($h\nu = 1486.7$ eV) sources. The total experimental uncertainty is equal to 0.15 and 0.56 eV respectively. These values are calculated considering the contribution of the source, which is of the order of few meV for UPS and equal to 0.35 eV for monochromatized Al source, and the one of the analyser, which is dependent on geometrical parameters of the analyser and pass energy [21]. In our XPS experimental condition it is not possible to resolve graphite sp^2 and CuPc benzenic signals. So, we cannot analyse the carbon spectra and they are not reported in this paper. Absolute energy calibration for UPS spectra was obtained by measuring the Fermi level of the metallic part of the molybdenum sample holder. XPS calibration was obtained by comparing the measured binding energy of C 1s peak with the reference value for graphite (BE = 284.5 eV) [22]. EELS experiments were conducted with a home-built monochromatic electron gun with a primary energy of $E_p = 91.5$ eV in specular reflection geometry. The angle between source and analyser is equal to 30°. Photoemission peaks were analysed using several Voigt profiles, with the constrain that the Gaussian full width at half maximum (FWHM) of peaks must be equal or greater than the experimental uncertainty. Some spectra were analysed with a global fitting procedure, that is all the spectra were analysed at the same time. This can be achieved considering that the χ^2 is equal to the sum of the individual spectra χ_i^2-like contributions. Each of them maximizes the likelihood function for its fitting function hypothesis. The individual contributions are correlated, sharing some of the fitting parameters, called global parameters. It follows that minimizing the sum of all the contributions allows for a simultaneous fit over the individual spectra, taking into account of their correlation and maximizing the likelihood function. We remark that global fitting procedure allows to use one guess function, which is common for all the spectra. Using the same home-built monochromatic electron gun of EELS, SA-LEED experiments were performed using $E_p = 33.1$ eV. Since positions of electron source and CHA are fixed, SA-LEED patterns were obtained by rotating the sample around the axis orthogonal to the scattering plane [17], defined as the plane containing the normal to sample surface, incident and scattered electron momenta. A SA-LEED pattern acquired with this technique explores a single direction of the reciprocal space. The others can be studied via an azimuthal rotation of the sample. The exchanged parallel momentum $\vec{q}$ was calibrated using the expected value for $G_{\Gamma M}$ peak of graphite [23], equal to 2.94 $Å^{-1}$.

3. Results and discussion

Fig. 1A reports a picture of 5 Å sample c-LEED pattern taken at 34.7 eV. We observe two bright circles at DK equal to about 0.45 and 1.0 $Å^{-1}$. We used a different diffraction technique to study the sample morphology, reported in Fig. 2. Indeed, when we perform SA-LEED, the transmission function is narrower and the signal to noise ratio is greater [13]. However, from c-LEED we can conclude that the system is azimuthally disordered. We explain this result considering that the HOPG is characterized by azimuthally disordered hexagonal terraces [19] and the phthalocyanine should grow along graphite high symmetry directions [6]. Consequently, we attribute the circular spots to CuPc with azimuthal disorder, which derives from the one of HOPG microcrystals. In Fig. 1B, we explain how circular spots are related to the primitive vectors of the reciprocal space lattice $\vec{a}$ and $\vec{b}$. Open circles are the points of the reciprocal space lattice, computed as $h\vec{a} + k\vec{b}$, where h and k are integers from 0 to infinity. Starting from those points the azimuthal disorder gives rise to a series of circles (dashed line), representing the place of points in the reciprocal space for which the diffraction conditions are satisfied. The bright circles in the diffraction pattern of Fig. 1A correspond to the dashed circles of Fig. 1B. Their radius is equal to the module of the vectors in reciprocal space. Therefore, there is a one by one correspondence between radius and the 2-D crystal structure. As stated before, we measure the diffraction patterns along a fixed azimuthal direction with SA-LEED, in order to obtain informations about cell parameters and the dimension of coherently scattering domains thanks to the greater resolution and sensitivity of this technique. Such measurements are reported in Fig. 2, they are obtained by acquiring the intensity of the elastic peak as a function of the exchanged parallel momentum along a fixed azimuthal direction i.e. the generic direction $\vec{d}$ of Fig. 1B. Then, these measurements are equal to the intensity profiles that would be measured along a

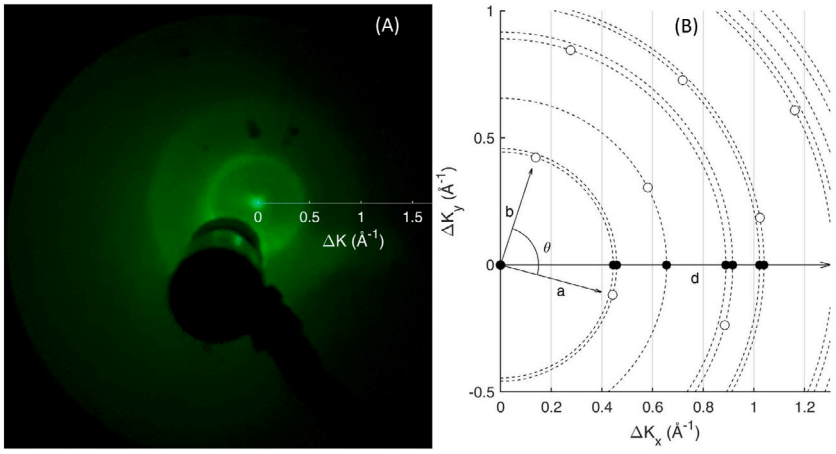

Fig. 1. (A) c-LEED pattern of 5 Å sample taken at 34.7 eV. The circular spots are attributed to the CuPc peak at 0.47 $Å^{-1}$ and to the two peaks at about 1 $Å^{-1}$, visible in Fig. 2. (B) Construction of peaks position in diffraction patterns. $\vec{a}$ and $\vec{b}$ are the primitive vectors of the reciprocal surface lattice and θ is the angle between them. Open circles are the points of the reciprocal lattice. The dashed circles represent the position of reciprocal lattice points resulting from the rotation of each point in every azimuthal direction. The SA-LEED measurements, reported in Fig. 2, were performed along a generic direction $\vec{d}$, where the reciprocal lattice points are projected (black dots).

diameter of c-LEED pattern circles, Fig. 1A. However, the different kinematic conditions and instruments characteristics allows to detect peaks, which were not observed in Fig. 1A, such as the one at about 0.66 $Å^{-1}$. In this way it is possible to determine the surface cell and the diameter of long-range ordered domains. The maxima in the diffraction patterns correspond to the intersection of the direction $\vec{d}$ with the dashed lines, that is when $q_{//}$ is equal to the module of the reciprocal surface vectors. The c-LEED pattern of Fig. 1A and the pattern in the middle of Fig. 2 have been measured from the same sample. The advantages of the latter method in terms of wave vector resolution and the dynamic of the signal intensity are clear. Moreover, SA-LEED operates with currents of only few tens of pA, which are significantly lower than the hundreds of nA used in c-LEED. This approach helps to prevent any damage to the sample due to electron bombardment.

In Fig. 2 we report the best fits of the SA-LEED patterns as a function of the sample thickness. The blue and green shaded peaks are attributed respectively to HOPG and CuPc signals. All CuPc peaks have the same width since they originate from the same structures. We observe a high diffuse background around the elastic peak (grey line), which is related to the vertical roughness of the sample [13], deriving from the island growth [9]. This background does not alter our analysis focused on position and width of CuPc and HOPG peaks since its contribution can be easily distinguished from the sharp peaks via the fitting procedure. The position of CuPc peaks can be calculated considering that the two primitive vectors in the reciprocal space are equal to $\vec{a} = a(1,0)$ and $\vec{b} = b(\cos\theta, \sin\theta)$, where a and b are the two primitive vectors module and θ is the angle between $\vec{a}$ and $\vec{b}$. Then, a generic point of reciprocal space lattice is $h\vec{a} + k\vec{b} = (ha + kb\cos\theta, kb\sin\theta)$. Due to the azimuthal disorder, we observe diffraction peaks when the exchanged parallel momentum is equal to the module of these reciprocal lattice points, see Fig. 1B, that is $|h\vec{a} + k\vec{b}| = \sqrt{(ha)^2 + 2kb\cos\theta \times ha + (kb\cos\theta)^2 + (kb\sin\theta)^2}$. The position of the calculated peaks depends on three parameters a,b and θ, which are optimized by the fitting procedure in order to minimize the distance between calculated and experimental peaks. This fit procedure is performed in Fourier space. The fit results are then transformed in real space coordinates: A and B, which are the modules of the vectors, and Θ, which is the angle between them. Fit results are reported in Table 2. The two thicker samples (5 Å and 33 Å) have the same surface structure, a parallelogram with a major angle of 93°. This structure is very close to the square cell reported in literature [9]. The best fit of 1.5 Å sample is obtained using the 5 Å one cell parameters. This model explains the peak appearing at 2.1 $Å^{-1}$. Then, it is a better representation of the experimental data than the one deriving from chains of molecules [6,8], which were observed in the very early stage of the growth.

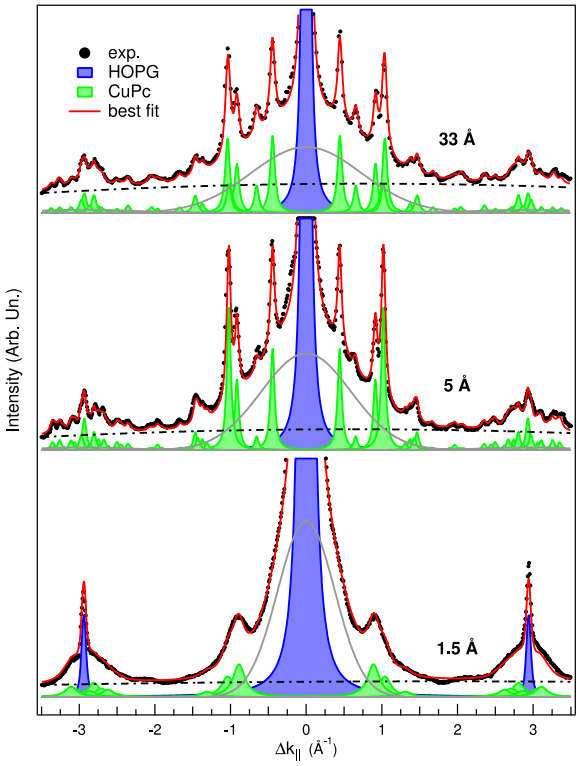

Fig. 2. Best fit of SA-LEED pattern of 33 Å (top), 5 Å (centre) and 1.5 Å (bottom) CuPc/HOPG samples. The green and blue shaded peaks correspond to the CuPc and HOPG signals respectively. The grey line around the elastic peak is due to the diffuse background. Fit parameters are reported in Table 2.

Table 2
Best values of fit parameters of SA-LEED patterns displayed in Fig. 2. t is sample thickness. A and B are the modules of real space surface vectors ($\vec{A} = 2\pi/\vec{a}$ and $\vec{B} = 2\pi/\vec{b}$). Θ is the angle between $\vec{A}$ and $\vec{B}$ vectors. Area is surface cell unit area $Area = \vec{A} \times \vec{B} = AB\sin(\Theta)$. D(CuPc) is the diameter of Pc long-range ordered domains.

t (Å)	A (Å)	B (Å)	Θ (°)	Area ($Å^2$)	D(CuPc) (Å)
1.5	14.15	13.74	93.12	194.15	44 ± 27
5	14.15 ± 0.04	13.74 ± 0.04	93.12 ± 0.30	194.15 ± 1.55	550 ± 110
33	14.05 ± 0.06	13.57 ± 0.03	92.89 ± 0.44	190.4 ± 2.3	420 ± 60

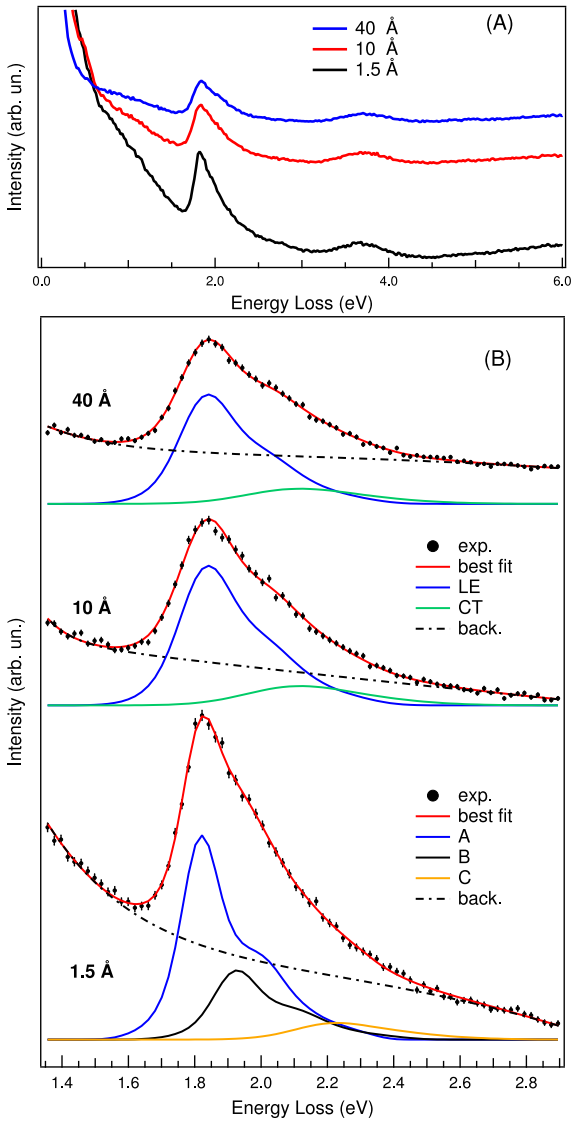

Fig. 3. (A) CuPc/HOPG EELS spectra as a function of sample thickness. In these spectra the Q band, at about 1.9 eV, and the B band (Soret band), at about 3.7 eV, are visible. The spectra are acquired in specular reflection geometry. The greater signal observed in 1.5 Å can be attributed to the greater graphite reflectivity than phthalocyanine one. Indeed, the intensity of elastic peak in 1.5 Å sample is 5 times the intensity of 40 Å one. (B) Q band best fit of 40 Å (top), 10 Å (centre) and 1.5 Å (bottom) CuPc/HOPG samples. LE and CT components, observed in 10 and 40 Å samples, are attributed to local excitations and charge transfer excitations. A two degrees polynomial plus a decreasing exponential is used to describe the background.

It is well known that the profile of the diffraction peaks carries information on the surface morphology and order extension [24]. For instance, the line shape associated to the formation of islands on a surface is a Lorentzian function [25] and its full width at half maximum (w) is related to the diameter of ordered domains with coherent scattering as $D = 4\pi/w$. The intrinsic line shape $I(\vec{q})$, where $\vec{q}$ is the exchanged parallel momentum, is broadened by the apparatus transmission function $T(\vec{q})$. Therefore, the measured line shape is equal to $J(\vec{q}) = I(\vec{q}) * T(\vec{q})$, where * indicates the convolution operation. The knowledge of the transmission function of our apparatus is a prerequisite for the determination of the dimension of surface domains of our samples. In order to determine the transmission function, we assume the HOPG as an ideal surface, whose intrinsic line shape of diffraction peak is equal to a delta function. In this case the measured diffraction peak corresponds to the transmission function of the apparatus. We measure and fit the specular peak of the clean HOPG sample. The best fit, representing the T function, is a Voigt line shape with a Gaussian

Table 3
Results of the global fitting procedure displayed in Fig. 3B. t is the sample thickness. For each component area, loss energy and Gaussian width (GW) are reported. Loss energies and Gaussian widths of LE and CT components are global parameters of 10 and 40 Å samples.

t (A)	Component	Area (A.U.)	Loss (eV)	GW (eV)
40	LE	1	1.835 ± 0.002	0.147 ± 0.010
	CT	0.256 ± 0.076	2.082 ± 0.031	0.297 ± 0.070
10	LE	1	1.835 ± 0.002	0.147 ± 0.010
	CT	0.197 ± 0.060	2.082 ± 0.031	0.297 ± 0.070
1	A	1	1.822 ± 0.009	0.093 ± 0.011
	B	0.37 ± 0.33	1.926 ± 0.028	0.116 ± 0.061
	C	0.122 ± 0.056	2.206 ± 0.033	0.224 ± 0.093

full width of $GW = (0.042 \pm 0.004)$ Å^{-1} and a Lorentzian one of $LW = (0.017 \pm 0.004)$ Å^{-1}. It is immediate to attribute the Gaussian broadening to the transmission function. Even if it is less evident, also the Lorentzian broadening could be associated to the transmission function. Indeed, the HOPG is characterized by a mosaic composed by ordered terraces with different orientation, which are not morphologically different from the aforementioned islands. The typical average dimension of these terraces is 1 μm [19]. Then, this sample should give rise to an intrinsic broadening of about 0.001 Å^{-1}, much smaller than the observed LW. In any case the measured LW of HOPG will be part of the uncertain associated to the CuPc long-range ordered domain size. The dimension of the ordered domains of samples with thickness equal to 5 and 33 Å is about 500 Å. This value is the first determination of long-range order of CuPc film using electron diffraction and it is greater than the one measured using STM for CuPc/Cu(111) (80 Å) [26] . This suggests that HOPG can favour the formation of an ordered film, as discussed later in this section. The dimension of the ordered domains for 1.5 Å sample is equal to 44 Å, much lower than the one of bulk phase. This is surprising, since the substrate template effect should be limited to the interface and, in principle, we could expect a greater 2-D order at CuPc/HOPG interface than in bulk phase. Moreover, the 2-D order on HOPG in bulk phase is much greater than the one on Al(100) in sub-monolayer phase [17]. These results will be discussed after the analysis of EELS and photoemission spectra.

In Fig. 3, we report the EELS spectra in the region of the so-called Q band (i.e. HOMO-LUMO transition) of the three samples with a nominal coverage of 1.5, 10 and 40 Å. The Q bands, as observed in these spectra, are quite different from the ones of the most common Pc molecular crystals. Indeed, the high energy shoulder is less intense with respect to the Q-band measured in the case of Pcs on Al(100), Au(110), InAs and InSb as for CuPc nanowires [3,27,28]. We fit the Q band to disentangle different electronic contributions and also to identify the Pc phase [3]. As highlighted by Feng et al. [15], the Davydov splitting is not adequate to describe the shape of the Q band and other processes have to be considered. In particular they shown that the splitting is due to electronic transitions between HOMO and LUMO of the same molecule (local excitations, LE) and of adjacent molecules (charge transfer excitations, CT). The relative weight of the LE and CT transitions depends on the Pc crystal structure as recently pointed out [18,29] and consequently to the grade of superposition of the HOMO and LUMO wave functions of the same molecule and of adjacent molecules. Both LE and CT components are simulated by a principal peak and vibronic satellites derived by the UV–Vis absorption spectrum of the isolated CuPc [30]. Since we assume that the nuclei wave function is not strongly modified by the presence of an extra electron or hole, we expect the same probability for vibronic excitations for both intra and extramolecular transitions. So, we use the same absorption spectrum for both LE and CT transitions. The absorption line shape is convoluted with a Gaussian function, which takes into account the instrumental broadening and the presence of inequivalent transitions with a similar energy [29]. In particular, calculated LE and CT excitations have a different energy spread [29] and, consequently, a different Gaussian width in our fitting procedure. The 10 and 40 Å samples EELS spectra are analysed jointly, see Table 3 for fit results. The

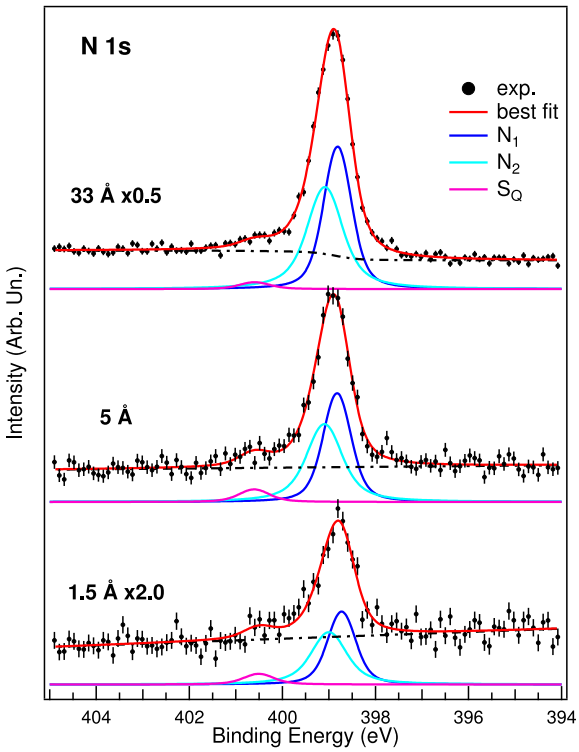

Fig. 4. Best fit of the N 1s level of 33 Å (top), 5 Å (centre) and 1.5 Å (bottom) CuPc/HOPG samples. The 33 Å and 1.5 Å spectra are multiplied for a constant, 0.5 and 2 respectively, to make easier the comparison. Nitrogen line shape is described by 3 components [31], called N_1, N_2 and S_Q. N_1 and N_2 are attributed to the two inequivalent nitrogen species of the molecule: N_1 is related to aza-bridge nitrogen and N_2 to pyrrolic nitrogen [32]. S_Q is a shake-up peak and its signal originates from HOMO-LUMO transitions associated to both nitrogen atoms [31,32].

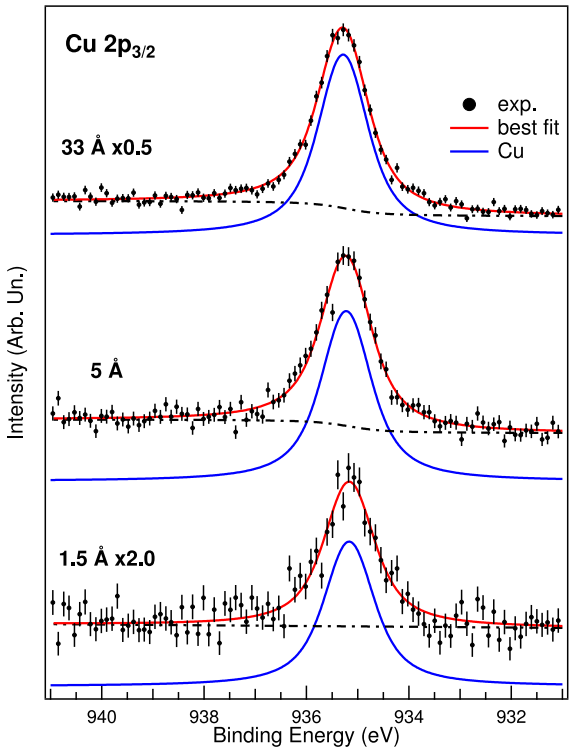

Fig. 5. Best fit of the Cu $2p_{3/2}$ level of 33 Å (top), 5 Å (centre) and 1.5 Å (bottom) CuPc/HOPG samples. The 33 Å and 1.5 Å spectra are multiplied for a constant, 0.5 and 2 respectively, to make easier the comparison. Copper spectra are characterized by only one peak, corresponding to copper in 2+ oxidation state, as was observed before in bulk phase molecules [16].

independent parameters are the areas of each peak, while the energy losses and widths are global parameters. Since the same ratio between CT and LE areas is obtained by the fitting procedure, both samples are in the same bulk phase. The same model cannot be applied to the 1.5 Å sample. Indeed, in this case we used 3 components (A,B and C), whose origin is discussed later. Since Q band line shape depends on the crystal phase, 1.5 Å sample has a different morphology with respect to the bulk one. As stated before, the Q bands of all the samples are different from the ones of the most common Pc phases [27], suggesting that the Pc on HOPG is in a characteristic phase. This particular crystal structure is the consequence of the molecule–substrate interaction. This interaction is studied via X-ray and ultraviolet photoemission spectroscopy. N 1s and Cu $2p_{3/2}$ photoemission spectra are measured as a function of the coverage, using a global fitting procedure for the spectra of samples of different thickness, Figs. 4 and 5. Cu $2p_{3/2}$ signal is composed by only one broad peak, due to Cu in 2+ oxidation state contained in the molecule [16].

N 1s spectra are fitted with three components associated to two inequivalent N atoms [32] (observed in the main peak and labelled N1 and N2), and to a shake-up excitation of HOMO-LUMO transition (the small peak labelled SQ) associated to both nitrogen atoms [31]. The best fit function of XPS spectra is obtained using the same intrinsic line shape for all coverages, i.e. each Lorentzian width, shift and ratio between components are equals. On the contrary, the overall shift of the whole lineshape, a multiplication constant and the gaussian widths are free parameters. However, no variations of Gaussian width are observed and only a global shift of (-0.13 ± 0.03) eV for copper and of (-0.095 ± 0.03) eV for nitrogen between 33 Å and 1.5 Å samples is measured. In Fig. 6 the UPS spectra of 33 Å, 5 Å and 1.5 Å CuPc/HOPG samples are reported in the binding energy region $0 \div 5$ eV.

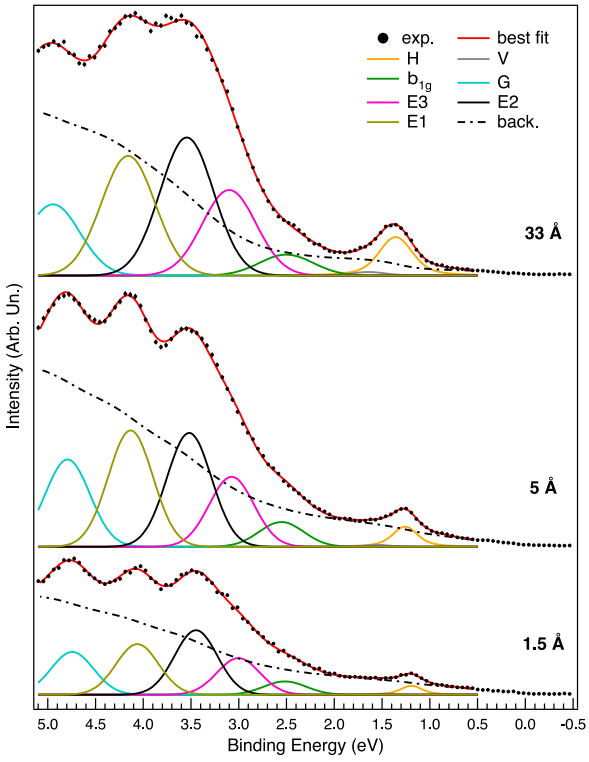

Fig. 6. Best fit of UPS spectra of 33 Å (top), 5 Å (centre) and 1.5 Å (bottom) CuPc/HOPG samples. The description of the components is reported in Section 3.

Also in this case a deconvolution of the experimental spectra is applied. The background is the sum of a Shirley background plus a line, which takes into account of the graphite signal, which is almost linear in this energy range. The peak at about 1.3 eV is fitted using two components (H and V) with the same width and ratio for all coverages, while the part of the spectrum between 2.5 and 4.8 eV is fitted with 5 components (b1g, E1, E2, E3, G). The peak at about 1.3 eV is due to the HOMO level and the C–C stretching excitations [33]. For this reason, H and V components are necessary to reproduce this part of the spectrum. b_{1g} component is attributed to the homonymous level [34]. G component corresponds to an electronic level localized on copper, nitrogen and benzenic carbon [35]. The components E1, E2 and E3 are attributed to levels that are mainly related to ligand [34,35], whose relative intensities depend on the orientation of the molecule [36]. The relative energy positions of E1, E2 and E3 are fixed for all coverages, while the absolute position is a free global parameter. No intensity variations are observed for different coverages. This suggests that the orientation of the molecule at the interface (1.5 Å sample) and in bulk phase (33 Å sample) is the same. Therefore, since the Pc adsorbs flat on graphite [6], Pc molecules are flat also in bulk phase [5,9]. The electronic structure of the molecules at the interface is not modified. Indeed, the only difference between bulk and interface molecules photoemission spectra is a little shift of about −0.1 eV of both valence and core levels peak. This shift is similar to the one observed for FePc/HOPG and it can be attributed to an image-charge screening [5]. This implies that molecules are weakly physisorbed and free to rearrange, giving rise to ordered 2-D islands [6]. However, the weak interaction between the molecule and the substrate is still stronger than the one between molecules. This is evident from the fact that heating at 500 °C the 5 Å sample gives rise to a partial desorption of CuPc film and a final coverage comparable with the one of the submonolayer 1.5 Å sample. To understand the sample morphology at the submonolayer phase, we have to take into account that chains, 2-D islands and 3-D islands arise as a function of monolayer completion and substrate temperature [6,8]. Moreover, a different Q band is expected for chains and 2-D crystals with respect to 3-D crystals one (observed in 10 and 40 Å samples), due to the impossibility of having transitions between adjacent molecules along the stacking axis [29]. From this, it follows that the presence of chains and 2-D and 3-D islands can explain the modifications of Q band line shape in sub-ML phase. Then, according to their energy, components A and C can be attributed respectively to LE and to 3-D islands CT excitations. Instead, B component should be related to unresolved LE and 3-D islands CT excitations. In this framework the much lower order at the interface can be explained with the contemporary presence of different structures: the 3-D crystals and almost square 2-D lattice as pointed out in this work; parallelogram 2-D lattice and chains of molecules as highlighted by STM [6]. All these structures contribute to the formation of the diffraction pattern. Since their contribution cannot be resolved, the 3-D peaks, observed in bulk phase, are broadened at the interface. In summary, Pcs are physisorbed on graphite, because no modifications of the electronic structure or charge transfer shifts are measured. The very weak interaction with HOPG let the physisorbed molecules free to move onto the substrate and rearrange via the side-by-side interaction [5]. Moreover, the Pcs adsorb on HOPG with a preferential flat orientation. Consequently, the molecules of the second layer can have a face-to-face interaction with the first layer one, facilitating the growth along a stacking axis. Since stacked molecules grow with the same flat orientation on a highly ordered 2-D basis, the bulk phase is ordered. On the contrary, at Pc/Al(100) interface the interaction is strong [16], therefore the rearrangement of adsorbed molecules is quenched, suppressing the formation of long-range ordered 2-D crystals [17]. Moreover, bulk growth on aluminium is characterized by molecules with the molecular plane almost perpendicular to the surface [16]. Indeed, the strong interaction, which modifies the electronic structure of the molecules at the interface, prevents the face-to-face interaction between the first two molecular layers. Then, in the second layer the molecules are probably decoupled from the substrate and they can stack freely in every direction parallel to the surface, giving rise to a high azimuthal disorder.

4. Conclusions

We have characterized the adsorption of CuPc molecules on HOPG using SA-LEED, EELS and photoemission spectroscopies. CuPc grows flat, forming in-plane long-range ordered domains. We attribute this result to a substrate templating effect, which favours a preferential flat orientation of the molecules, increases the bidimensional order of the system and facilitates the molecular self-assembly of the molecule along a stacking axis. In this way, Pcs form coherently scattering domains with a diameter of 500 Å. The ordered bulk growth is possible as a consequence of the weak interaction between physisorbed molecules and substrate, which does not modify the electronic structure of interface molecules. Indeed, no significant variations of the line shapes are measured with photoemission spectroscopy as a function of the coverage. The only difference between thick and 1.5 Å sample is a rigid shift of peaks (−0.1 eV), which can be attributed to a pure image-charge screening [5].

CRediT authorship contribution statement

Daniele Paoloni: Conceptualization, Methodology, Software, Validation, Formal analysis, Investigation, Resources, Data curation, Writing – original draft, Writing - review & editing, Visualization. **Alessandro Ruocco:** Conceptualization, Methodology, Software, Validation, Formal analysis, Investigation, Resources, Data curation, Writing – original draft, Writing – review & editing, Visualization, Supervision, Funding acquisition.

Declaration of competing interest

The authors declare that they have no known competing financial interests or personal relationships that could have appeared to influence the work reported in this paper.

Data availability

Data will be made available on request.

Acknowledgements

Partial financial support by Università degli Studi Roma Tre, Italy, Piano Straordinario della Ricerca 2015, azione n. 3 -Potenziamento dei laboratori di ricerca- is greatly acknowledged.

References

[1] C.D. Dimitrakopoulos, D.J. Mascaro, Organic thin-film transistors: A review of recent advances, IBM J. Res. Dev. 45 (1) (2001) 11–27, http://dx.doi.org/10.1147/rd.451.0011.

[2] S.A. Choi, K. Kim, S.J. Lee, H. Lee, A. Babajanyan, B. Friedman, K. Lee, Effects of thermal preparation on Copper Phthalocyanine organic light emitting diodes, J. Lumin. 171 (2016) 149–153, http://dx.doi.org/10.1016/j.jlumin.2015.11.015, URL https://www.sciencedirect.com/science/article/pii/S002223131530586X.

[3] G.M. Pierantozzi, M. Sbroscia, A. Ruocco, Templating effect of the substrate on the structure of Cu-phthalocyanine thin film, Surf. Sci. 669 (2018) 176–182, http://dx.doi.org/10.1016/j.susc.2017.12.003, URL https://linkinghub.elsevier.com/retrieve/pii/S0039602817306647.

[4] D.G. de Oteyza, A. El-Sayed, J.M. Garcia-Lastra, E. Goiri, T.N. Krauss, A. Turak, E. Barrena, H. Dosch, J. Zegenhagen, A. Rubio, Y. Wakayama, J.E. Ortega, Copper-phthalocyanine based metal–organic interfaces: The effect of fluorination, the substrate, and its symmetry, J. Chem. Phys. 133 (21) (2010) 214703, http://dx.doi.org/10.1063/1.3509394, URL https://aip.scitation.org/doi/abs/10.1063/1.3509394, Publisher: American Institute of Physics.

[5] C. Isvoranu, J. Åhlund, B. Wang, E. Ataman, N. Mårtensson, C. Puglia, J.N. Andersen, M.-L. Bocquet, J. Schnadt, Electron spectroscopy study of the initial stages of iron phthalocyanine growth on highly oriented pyrolitic graphite, J. Chem. Phys. 131 (21) (2009) 214709, http://dx.doi.org/10.1063/1.3259699, URL https://aip.scitation.org/doi/10.1063/1.3259699.

[6] J. Åhlund, J. Schnadt, K. Nilson, E. Göthelid, J. Schiessling, F. Besenbacher, N. Mårtensson, C. Puglia, The adsorption of iron phthalocyanine on graphite: A scanningfff tunnelling microscopy study, Surf. Sci. 601 (17) (2007) 3661–3667, http://dx.doi.org/10.1016/j.susc.2007.06.008, URL https://linkinghub.elsevier.com/retrieve/pii/S0039602807006346.

[7] C. Ludwig, Epitaxy and scanning tunneling microscopy image contrast of copper–phthalocyanine on graphite and MoS2, J. Vac. Sci. Technol. B 12 (3) (1994) 1963, http://dx.doi.org/10.1116/1.587680, URL http://scitation.aip.org/content/avs/journal/jvstb/12/3/10.1116/1.587680.

[8] K. Walzer, M. Hietschold, STM and STS investigation of ultrathin tin phthalocyanine layers adsorbed on HOPG(0001) and Au(111), Surf. Sci. 471 (1) (2001) 1–10, http://dx.doi.org/10.1016/S0039-6028(00)00909-2, URL https://www.sciencedirect.com/science/article/pii/S0039602800009092.

[9] S.D. Wang, X. Dong, C.S. Lee, S.T. Lee, Orderly growth of copper phthalocyanine on highly oriented pyrolytic graphite (HOPG) at high substrate temperatures, J. Phys. Chem. B 108 (5) (2004) 1529–1532, http://dx.doi.org/10.1021/jp0361733, URL https://pubs.acs.org/doi/10.1021/jp0361733.

[10] I.V. Bondarev, A. Popescu, R.A. Younts, B. Hoffman, T. McAfee, D.B. Dougherty, K. Gundogdu, H.W. Ade, Lowest energy frenkel and charge transfer exciton intermixing in one-dimensional copper phthalocyanine molecular lattice, Appl. Phys. Lett. 109 (21) (2016) 213302, http://dx.doi.org/10.1063/1.4968821, arXiv:https://doi.org/10.1063/1.4968821.

[11] E. del Pino Rosendo, O. Yildiz, W. Pisula, T. Marszalek, P.W. Blom, C. Ramanan, Symmetry-breaking charge transfer and intersystem crossing in copper phthalocyanine thin films, Phys. Chem. Chem. Phys. 25 (9) (2023) 6847–6856.

[12] R. Kraus, M. Grobosch, M. Knupfer, Full electronic excitation spectrum of condensed manganese phthalocyanine, Chem. Phys. Lett. 469 (1–3) (2009) 121–124.

[13] M.H.-v. Hoegen, Growth of semiconductor layers studied by spot profile analysing low energy electron diffraction–part I 1, Z. Kristallogr.-Crystal. Mater. 214 (10) (1999) 591–629.

[14] C. Fandaruff, M.A. Segatto Silva, D.C. Galindo Bedor, D.P. de Santana, H.V.A. Rocha, L. Rebuffi, C.L. Azanza Ricardo, P. Scardi, S.L. Cuffini, Correlation between microstructure and bioequivalence in Anti-HIV drug efavirenz, Eur. J. Pharmaceut. Biopharmaceut. 91 (2015) 52–58, http://dx.doi.org/10.1016/j.ejpb.2015.01.020, URL https://www.sciencedirect.com/science/article/pii/S0939641115000363.

[15] J.H. Park, J.E. Royer, E. Chagarov, T. Kaufman-Osborn, M. Edmonds, T. Kent, S. Lee, W.C. Trogler, A.C. Kummel, Atomic imaging of the irreversible sensing mechanism of NO2 adsorption on copper phthalocyanine, J. Am. Chem. Soc. 135 (39) (2013) 14600–14609, http://dx.doi.org/10.1021/ja403752r, arXiv:https://doi.org/10.1021/ja403752r, PMID: 23968338.

[16] A. Ruocco, F. Evangelista, R. Gotter, A. Attili, G. Stefani, Evidence of charge transfer at the Cu-phthalocyanine/Al(100) interface, J. Phys. Chem. C 112 (6) (2008) 2016–2025, http://dx.doi.org/10.1021/jp076299q.

[17] D. Paoloni, G. Di Filippo, D. Cvetko, G. Kladnik, A. Morgante, A. Ruocco, Strong chemical interaction and self-demetalation of Zinc-Phthalocyanine on Al(100), J. Phys. Chem. C 124 (41) (2020) 22550–22558, http://dx.doi.org/10.1021/acs.jpcc.0c06980, URL https://pubs.acs.org/doi/10.1021/acs.jpcc.0c06980.

[18] S. Feng, Y.-C. Wang, Y. Ke, W. Liang, Y. Zhao, Effect of charge-transfer states on the vibrationally resolved absorption spectra and exciton dynamics in ZnPc aggregates: Simulations from a non-Makovian stochastic Schrödinger equation, J. Chem. Phys. 153 (3) (2020) 034116, http://dx.doi.org/10.1063/5.0013935, URL https://aip.scitation.org/doi/abs/10.1063/5.0013935.

[19] A.W. Moore, Highly oriented pyrolytic graphite, 1973.

[20] C.S. Fadley, Electron Spectroscopy Theory Techniques and Applications, Academic Press, 1978.

[21] J.H. Moore, C.C. Davis, M.A. Coplan, S.C. Greer, Building Scientific Apparatus, fourth ed., Cambridge University Press, 2009, http://dx.doi.org/10.1017/CBO9780511609794.

[22] K.L. Smith, K.M. Black, Characterization of the treated surfaces of silicon alloyed pyrolytic carbon and SiC, J. Vac. Sci. Technol. A 2 (2) (1984) 744–747, http://dx.doi.org/10.1116/1.572562, URL https://avs.scitation.org/doi/abs/10.1116/1.572562.

[23] A. Bellissimo, G.M. Pierantozzi, A. Ruocco, G. Stefani, O.Y. Ridzel, V. Astašauskas, W.S. Werner, M. Taborelli, Secondary electron generation mechanisms in carbon allotropes at low impact electron energies, J. Electron Spectrosc. Relat. Phenom. 241 (2020) 146883, http://dx.doi.org/10.1016/j.elspec.2019.07.004, URL https://linkinghub.elsevier.com/retrieve/pii/S0368204819300039.

[24] M. Henzler, LEED studies of surface imperfections, Appl. Surf. Sci. 11–12 (1982) 450–469, http://dx.doi.org/10.1016/0378-5963(82)90092-7, URL https://linkinghub.elsevier.com/retrieve/pii/0378596382900927.

[25] J. Wollschläger, F. Schäfer, K. Schröder, Diffraction spot profile analysis for vicinal surfaces with long-range order, Surf. Sci. 396 (1–3) (1998) 94–106, http://dx.doi.org/10.1016/S0039-6028(97)00662-6, URL https://linkinghub.elsevier.com/retrieve/pii/S0039602897006626.

[26] T. Stock, J. Nogami, Copper phthalocyanine thin films on Cu(111): Submonolayer to multi-layer, Surf. Sci. 637–638 (2015) 132–139, http://dx.doi.org/10.1016/j.susc.2015.03.028, URL https://www.sciencedirect.com/science/article/pii/S0039602815000886.

[27] H. Wang, S. Mauthoor, S. Din, J.A. Gardener, R. Chang, M. Warner, G. Aeppli, D.W. McComb, M.P. Ryan, W. Wu, A.J. Fisher, M. Stoneham, S. Heutz, Ultralong copper phthalocyanine nanowires with new crystal structure and broad optical absorption, ACS Nano 4 (7) (2010) 3921–3926, http://dx.doi.org/10.1021/nn100782w.

[28] E. Salomon, T. Angot, N. Papageorgiou, J.-M. Layet, Adsorption of metal-free phthalocyanine on InSb and InAs(001)-4 × 2/c(8 × 2) surface, J. Phys. Chem. C 111 (15) (2007) 5721–5725, http://dx.doi.org/10.1021/jp0663356, arXiv:https://doi.org/10.1021/jp0663356.

[29] S. Feng, Y.-C. Wang, W. Liang, Y. Zhao, Vibrationally resolved absorption spectra and exciton dynamics in zinc phthalocyanine aggregates: Effects of aggregation lengths and remote exciton transfer, J. Phys. Chem. A 125 (14) (2021) 2932–2943, http://dx.doi.org/10.1021/acs.jpca.1c01271.

[30] A. Aktaş Kamiloğlu, D. Akyüz, A. Koca, r. Acar, Synthesis and investigation of spectroelectrochemical properties of peripherally tetra-substituted phthalocyanine bearing 3-(4-{[3-(trifluoromethyl)benzyl]oxy}phenyl)propan-1-ol and its metallo compounds, J. Incl. Phenom. Macrocycl. Chem. 92 (1–2) (2018) 223–235, http://dx.doi.org/10.1007/s10847-018-0837-6, URL http://link.springer.com/10.1007/s10847-018-0837-6.

[31] F. Evangelista, A. Ruocco, R. Gotter, A. Cossaro, L. Floreano, A. Morgante, F. Crispoldi, M.G. Betti, C. Mariani, Electronic states of CuPc chains on the Au(110) surface, J. Chem. Phys. 131 (17) (2009) 174710, http://dx.doi.org/10.1063/1.3257606.

[32] M.V. Nardi, F. Detto, L. Aversa, R. Verucchi, G. Salviati, S. Iannotta, M. Casarin, Electronic properties of CuPc and H2Pc: an experimental and theoretical study, Phys. Chem. Chem. Phys. 15 (31) (2013) 12864, http://dx.doi.org/10.1039/c3cp51224j, URL http://xlink.rsc.org/?DOI=c3cp51224j.

[33] S. Kera, H. Fukagawa, T. Kataoka, S. Hosoumi, H. Yamane, N. Ueno, Spectroscopic evidence of strong $\pi - \pi$ interorbital interaction in a lead-phthalocyanine bilayer film attributed to the dimer nanostructure, Phys. Rev. B 75 (12) (2007) 121305, http://dx.doi.org/10.1103/PhysRevB.75.121305, URL https://link.aps.org/doi/10.1103/PhysRevB.75.121305.

[34] F. Evangelista, V. Carravetta, G. Stefani, B. Jansik, M. Alagia, S. Stranges, A. Ruocco, Electronic structure of copper phthalocyanine: An experimental and theoretical study of occupied and unoccupied levels, J. Chem. Phys. 126 (12) (2007) 124709, http://dx.doi.org/10.1063/1.2712435, _eprint:.

[35] V.Y. Aristov, O.V. Molodtsova, V. Maslyuk, D.V. Vyalikh, V.M. Zhilin, Y.A. Ossipyan, T. Bredow, I. Mertig, M. Knupfer, Electronic structure of pristine CuPc: Experiment and calculations, Appl. Surf. Sci. 254 (1) (2007) 20–25, http://dx.doi.org/10.1016/j.apsusc.2007.07.096, URL https://www.sciencedirect.com/science/article/pii/S0169433207009087.

[36] T. Toader, G. Gavrila, W. Braun, J. Ivanco, D.R.T. Zahn, Valence band fine structure of copper phthalocyanine thin films: Effect of molecular orientation, Phys. Status Solidi (B) 246 (7) (2009) 1510–1518, http://dx.doi.org/10.1002/pssb.200945141, URL https://onlinelibrary.wiley.com/doi/abs/10.1002/pssb.200945141.